Reflectance anisotropy of GaAs(100): Dislocation-induced piezo-optic effects

L. F. Lastras-Martínez and A. Lastras-Martínez

Instituto de Investigación en Comunicación Optica, Universidad Autónoma de San Luis Potosí,
Alvaro Obregón 64, San Luis Potosí, Mexico

We develop a model to describe reflectance-difference (RD) spectra of zinc-blende semiconductors due to strains induced by α and β 60° dislocations. It is shown that near the semiconductor surface, as a result of the lost of lattice periodicity, dislocations result in an anisotropic average strain that changes the symmetry from cubic to orthorhombic, thus leading to a reflectance anisotropy. We obtain expressions for RD spectra at critical points of both Γ and Λ symmetry that predict first-derivative RD line shapes as long as the strain-induced energy shifts are small compared to spectra broadening energies. Furthermore, we report on RD spectra of semi-insulating GaAs (100) in the 1.2–5.5-eV energy range and show that such spectra comprise a component that is well described by our model. [S0163-1829(96)09239-9]

I. INTRODUCTION

Reflectance-difference spectroscopy[1] (RDS) has emerged in recent years as a sensitive optical probe for the characterization of a number of optical processes in cubic semiconductors. Among the applications of RDS, we can mention the in situ, real time, monitoring of epitaxial growth processes in both molecular-beam epitaxy[2] and metalorganic chemical-vapor-deposition (MOCVD) reactors,[3] and the in situ determination of doping levels of epitaxial layers grown by MOCVD.[4] Because of its broad range of applications, much theoretical and experimental work has been dedicated to clarifying the physical mechanisms responsible for the observed reflectance anisotropies. Such work has been carried out in Si,[5,6] Ge,[6,7] GaAs,[8] and InP,[8] among other semiconductors. Despite this effort, however, the mechanisms giving rise to an anisotropic interaction of the light with the semiconductor surface are only partially understood at present. Indeed, while it seems straightforward to conclude that the breakdown of the cubic symmetry near the semiconductor surface should lead to surface anisotropies, experiment shows that RD spectra are rather complex, comprising several components with various physical origins. In this regard, RD spectra have been reported to include components due to local-field effects,[6,7] surface reconstruction,[9] molecule adsorption,[5] spatial dispersion,[8] and both linear[10] and quadratic[11] electro-optic effects.

In a previous paper, we have reported that, in addition to all the above mechanisms, RD spectra comprise components associated with the strain induced by 60° α and β dislocations.[12] The results of Ref. 12 make it possible for RDS to be used in the characterization of dislocations in semiconductors. In this paper, we develop a model to explain dislocation-induced RD line shapes. This model is based on dislocation-induced piezo-optic effects. We consider both Γ- and Λ-point interband transitions and extend the experimental results of Ref. 12 to include the E'_0, $E'_0+\Delta'_0$, and $E'_0+\Delta'_0+\Delta_0$ critical-point transitions.

II. EXPERIMENT

A. Experimental procedure

The RD measurements were performed on commercial Cr-doped semi-insulating GaAs crystals oriented in the (100) direction. We used semi-insulating samples in order to avoid the electro-optic effects that are known to dominate the GaAs RD spectra around the E_1 and $E_1+\Delta_1$ transitions for both n- and p-type crystals.[13] Such electro-optic effects are associated with the surface electric field due to surface band bending. Because of its high resistivity, no appreciable electro-optic effects are expected for Cr-doped GaAs.

The spectrometer employed in this work for the RD measurements is schematically shown in Fig. 1. In this setup, light coming from either a Xe lamp or a Tungsten lamp is focused at the entrance slit of a 0.25-m monochromator. Two 50-cm focal length mirrors direct the light beam at the output of the monochromator through a polarizer prism (quartz Rochon) and a photoelastic modulator (Hinds Instruments, model PEM-80) and focuses it on the sample surface with an angle of incidence of about 10°. The polarizer prism and photoelastic modulator in tandem allow for the polarization of the light incident on the sample surface to be modulated at a frequency of 50 kHz between two orthogonal, linearly polarized states. For the experiment, the sample is aligned so that the two extreme polarization states coincide with the sample optical axis [0$\bar{1}$1] and [011] directions. Upon reflec-
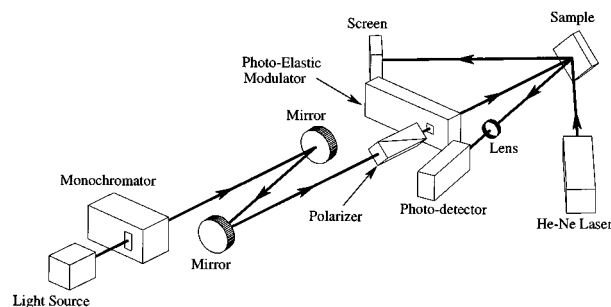
FIG. 1. Schematics of the spectrometer employed for the reflectance-difference measurements.
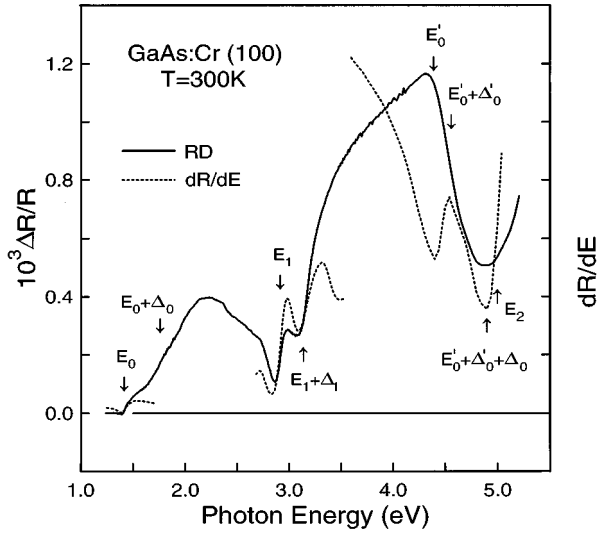
FIG. 2. Reflectance-difference spectrum for GaAs:Cr (100) in the 1.2–5.5-eV energy range.

FIG. 3. Geometry and classification of 60° dislocations. (a) Burgers vector **b** and its edge (**b**$_e$) and screw (**b**$_s$) components for an α^+ dislocation. Vectors **b**, **b**$_e$, and **b**$_s$ lie on plane (111), while **b** is directed along [110], making an angle of 60° with dislocation core **l**. (b) Burgers vector orientations for (α^+,β^-) and (α^-,β^+) dislocations.

tion, the light beam is focused on the active area of a UV-enhanced silicon photodetector whose electric output is fed to a lock-in amplifier tuned to twice the photoelastic modulator frequency. The spectrometer operates in the 1.2–5.5-eV energy range. More experimental details can be found elsewhere.[14]

To suppress parasitic signals in the measured RD spectra, we have employed the procedure described in Ref. 14 that consists in measuring two spectra with sample azimuthal orientations $\pi/2$ radians apart and then subtracting them. To facilitate the two measurements, the sample is mounted on two rotating discs joined by a spring and three adjusting screws. This arrangement, together with a He-Ne laser impinging on the sample, allows the sample surface to be aligned perpendicularly to the rotation axis.

B. Experimental results

In Fig. 2 we show a (100) GaAs:Cr typical spectrum in the 1.2–5.5-eV energy range, obtained as describe above. On top of a relatively structureless background, we can see prominent structures around the E_1 and $E_1+\Delta_1$ transition energies (2.91 and 3.13 eV, respectively) as well as around the E_0' triplet (4.2–5.0 eV). A smaller but well defined structure is also seen around the fundamental gap E_0. In contrast, no appreciable structure is observed around the $E_0+\Delta_0$ transition, a feature that will be discussed below. Broken lines around critical points in Fig. 2 correspond to the numerical energy derivative dR/dE of the GaAs reflectivity. The coinciding of the broken line spectra with the RD line shape is indicative of the existence of a first-derivative component in the RD spectra.[12] We note, however, that the relationship between the RD and dR/dE line shapes is not a simple one, since the various critical points contribute to RD spectra with characteristic relative amplitudes and phases that are different from those for the corresponding dR/dE line shapes, as discussed below.

As previously reported,[12] the first-derivative RD spectrum of Fig. 2 is associated with an anisotropic surface strain that

changes the GaAs symmetry near the surface from cubic (point group T_d) to orthorhombic (point group C_{2v}). Such stress is generated by the edge component of α and β 60° dislocations, provided that the density of one of them dominates over that of the other. In the next section, we will discuss an RD line-shape model based on the average strain due to the difference in the densities of α and β dislocations that normally occurs in GaAs.[15,16]

III. THEORETICAL MODEL

A. Geometry of 60° dislocations

To discuss dislocation-induced strains and associated optical anisotropies, we will consider the coordinate axis (x,y,z) defined in Fig. 3(a). We will assume normal light incidence on the (100) surface of GaAs, and we will be interested in anisotropies occurring along this surface.

Sixty-degree dislocations are known to be a common occurrence in zinc-blende crystals.[16,17] Such dislocations, which are characterized by the fact that the Burgers vector makes an angle of 60° with the dislocation core **l** (which lies along any of the six equivalent $\langle 011\rangle$ directions), have both screw and edge components that are directed along the $\langle 011\rangle$ and $\langle 211\rangle$ directions, respectively. In Fig. 3(a) the geometry of 60° dislocations is illustrated for the particular case of a dislocation with a core **l** along $[0\bar{1}1]$ and edge and screw Burgers vector components along $[2\bar{1}1]$ and $[01\bar{1}]$, respectively, leading to a total Burgers vector along [101].

The crystallographic orientation of both components of the Burgers vector, displays 48 types of 60° dislocations.[16,17] In what follows, however, we will consider only the 16 dislocations with cores oriented along $[01\bar{1}]$ or [011], since they are the only ones leading to an optical anisotropy for normal incidence on the (100) surface, as can be easily verified from symmetry considerations. Burgers vectors for these sixteen dislocations are given by

$$\mathbf{b}^{(ijkmn)}=\mathbf{b}_e^{(ijk)}+\mathbf{b}_s^{(mn)}=-\frac{a}{4}[ijk]+\frac{a}{4}[0mn], \quad (1)$$

where a is the unit cell parameter and subscripts e and s stand for the edge and screw components of the Burgers

TABLE I. Conventions used in this paper for the indices $ijkmn$ of the 16 60° dislocations with cores parallel to the (100) surface ($i=\pm2$). Indices (j,k,i) and (m,n) determine the orientations of the edge and screw components of the Burgers vector, respectively. Dislocation type and sign are determined by indices j and k, respectively.

Dislocation type	b_e			b_s	
	j	k	i	m	n
α^+	1	1	2	±1	∓1
			-2	∓1	±1
α^-	1	-1	2	±1	±1
			-2	∓1	∓1
β^+	-1	1	2	±1	±1
			-2	∓1	∓1
β^-	-1	-1	2	±1	∓1
			-2	∓1	±1

vector, respectively. Index i takes values ±2, while j, k, m, and n take values ±1, provided that the condition $|l\cdot b| =lb\cos(\pi/3)$ is fulfilled. In Table I we resume the possible indicator combinations.

60° dislocations are termed α or β according to whether their cores are composed of arsenic or gallium atoms, respectively.[16] Furthermore, 60° dislocations can be negative or positive depending on whether the dislocation extra half plane is introduced from the surface toward the interior of the crystal or in the opposite direction. The dislocation type (α^+, α^-, β^+, or β^-) is determined by the value of indices j and k as indicated in Table I. In Fig. 3(b) we illustrate the geometry of the sixteen 60° dislocations defined by Eq. (1). We note that cores of $\alpha(\beta)$ dislocations of a given sign are rotated 90° with respect to cores of $\beta(\alpha)$ dislocations of the same sign, while cores of positive and negative dislocations of the same type (either α or β) are rotated 90° with respect to each other.

B. Strain tensor for 60° dislocations

The strain tensor for the edge components of the dislocations defined by Eq. (1) can be obtained by the procedure outlined by Eshelby, Read, and Shockley.[18] Such a tensor is a function of three independent parameters e_{11}, e_{12}, and e_{22}, and can be written

$$\mathbf{e}^{(ijk)}_{(e)}=\frac{1}{2}\begin{bmatrix} 2ke_{11} & ij\delta_{jk}e_{12} & ij(\delta_{jk}-1)e_{12} \\ ij\delta_{jk}e_{12} & 2j\delta_{jk}e_{22} & 0 \\ ij(\delta_{jk}-1)e_{12} & 0 & 2j(\delta_{jk}-1)e_{22} \end{bmatrix}. \quad (2a)$$

In Fig. 4 we illustrate the strain field described by tensor (2a) for dislocations α^+, α^-, and β^-. Lines within circles around dislocations represent the resulting elastic deformation of an otherwise cubic lattice. We note that dislocation strain fields include tension (shaded areas) as well as compression (unshaded areas) domains.

The screw component tensor, on the other hand, is a function of two parameters, e_{13} and e_{23}, and is written as follows:
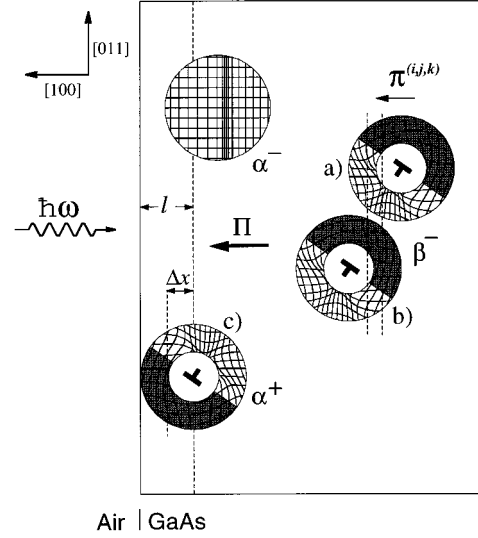
FIG. 4. Strain fields due to 60° dislocations. Lines around dislocation cores represent the dislocation-induced strains in an otherwise cubic lattice.

$$\mathbf{e}^{(mn)}_{(s)}=\begin{bmatrix} 0 & \delta_{mn}e_{13} & (1-\delta_{mn})e_{13} \\ \delta_{mn}e_{13} & 0 & -ne_{23} \\ (1-\delta_{mn})e_{13} & -ne_{23} & 0 \end{bmatrix}. \quad (2b)$$

Taking into account that we are considering only linear piezo-optic contributions to the RD spectra, we will model the strain induced by a dislocation by making it equal to the strain average over a plane parallel to the (100) surface

$$\langle\mathbf{e}_{(e,s)}\rangle=\frac{1}{2l^2}\left[\int_{z_0-l/2}^{l/2+z_0}\int_{y_0-l}^{l+y_0}\mathbf{e}_{(e,s)}dydz\right]_{x=x_0+\Delta x}, \quad (3)$$

where (x_0,y_0,z_0) is the dislocation center, l is the dislocation radius of influence whose magnitude will be assumed to be equal to the magnitude of the dislocation length,[19] and $\Delta x\approx l/2$ (see Fig. 4).

To obtain the average strain tensors, we note that for the stress tensor component τ_{11} we have $\langle\tau_{11}\rangle=0$, so that we can write

$$\langle e_{11}\rangle=-\frac{c_{12}}{c_{11}}\langle e_{22}\rangle. \quad (4)$$

Furthermore, as the average value of τ_{12} also vanishes, we have

$$\langle e_{12}\rangle=\langle e_{21}\rangle=0. \quad (5)$$

Equations (2)–(5) lead to the average strain tensors

$$\langle\mathbf{e}^{(ijk)}_{(e)}\rangle=\langle e_{22}\rangle\begin{pmatrix} -k\dfrac{c_{12}}{c_{11}} & 0 & 0 \\ 0 & j\delta_{jk} & 0 \\ 0 & 0 & j(\delta_{jk}-1) \end{pmatrix}, \quad (6a)$$

and

$$\langle \mathbf{e}^{(mn)}_{(s)} \rangle = -n\langle e_{23} \rangle \begin{pmatrix} 0 & 0 & 0 \\ 0 & 0 & 1 \\ 0 & 1 & 0 \end{pmatrix}. \tag{6b}$$

We note that tensors (6a) and (6b) depend only on the parameters e_{22} and e_{23}, respectively.

C. Anisotropic strains due to 60° dislocations

Tensors (6a) and (6b), which are dependent of $x-x_0$, describe the strain associated with a single dislocation. We note that such a strain results in local anisotropy for light incident along the (100) surface. Any reflection anisotropy, however, results from the average contributions of all dislocations present within the light-penetration depth into the semiconductor. Regarding this, we note that although the strain contributions of dislocations in the semiconductor bulk average out to zero, near the surface, as a result of the loss of lattice periodicity, dislocations may lead to a crystal anisotropy. To be more specific, the average strain contributions of tensor (6b) are always zero, even near the surface; tensor (6a), on the other hand, would lead to an anisotropically stressed surface layer of thickness $\approx l$ provided that there is a difference in the density of α and β dislocations.

The above comments may be understood if we consider pairs of identical dislocations displaced with respect to each other perpendicularly to the semiconductor surface by a distance approximately equal to the dislocation radius of influence l, as is schematically shown by dislocations (a) and (b) in Fig. 4. As is clear from this figure, the tension domain of dislocation (a) averages out to zero with the compression domain of dislocation (b), thus leading to a zero average strain field. Such a pairing of dislocations, however, is not possible for dislocations within a surface layer of thickness of the order of l, as is evident for dislocation (c) in Fig. 4, thus allowing for dislocations to generate a surface anisotropy.

Taking into account that the relevant parameter for reflectance anisotropies is $\langle e_{22} \rangle$ and that it is an odd function of $x-x_0$ that describes tension as well as compression domains, the above discussion can be stated in a formal way by defining, in analogy with electric-polarization phenomena, an "anisotropic strain dipole" for dislocation $ijkmn$ by

$$\boldsymbol{\pi}^{(ijkmn)} = \Delta e^{(ijkmn)} \mathbf{l}, \tag{7}$$

where $\mathbf{l}$ is defined to be perpendicular to the surface (100) (see Fig. 4) and

$$\Delta e^{(ijkmn)} = \hat{\mathbf{e}}_z \cdot [\langle \mathbf{e}^{(ijk)}_{(e)} \rangle + \langle \mathbf{e}^{(mn)}_{(s)} \rangle] \cdot \hat{\mathbf{e}}_z$$
$$- \hat{\mathbf{e}}_y \cdot [\langle \mathbf{e}^{(ijk)}_{(e)} \rangle + \langle \mathbf{e}^{(mn)}_{(s)} \rangle] \cdot \hat{\mathbf{e}}_y, \tag{8}$$

where $\hat{\mathbf{e}}_y$ and $\hat{\mathbf{e}}_z$ are unit vectors along y and z, respectively. $\Delta e^{(ijkmn)}$ corresponds to the difference in strain along y and z due to dislocation $ijkmn$.

We will also define an "anisotropic strain polarization" field by the relation

$$\boldsymbol{\Pi} = \sum_{ijkmn} \rho^{(ijkmn)} \boldsymbol{\pi}^{(ijkmn)}, \tag{9}$$

where $\rho^{(ijkmn)}$ is the volume density for dislocation $ijkmn$. Furthermore, by carrying out the summation over $ijkmn$ in Eq. (9) by employing tensors (6a) and (6b) we obtain

$$\boldsymbol{\Pi} = \langle e_{22} \rangle l \Delta\rho, \tag{10}$$

where $\Delta\rho = \rho^{\alpha} - \rho^{\beta}$ is the difference between α and β dislocation densities. On the other hand, by assuming a uniform dislocation distribution, the Π vector should satisfy the relation

$$\oint_s \boldsymbol{\Pi} \cdot d\boldsymbol{\sigma} = 0, \tag{11}$$

where integration is carried out on a surface enclosing a large enough number of dislocations.

From Eqs. (10) and (11) we finally obtain for the difference in average strain per unit area along y and z

$$\Delta e = \boldsymbol{\Pi} \cdot \hat{\mathbf{n}} = \langle e_{22} \rangle l \Delta\rho, \tag{12}$$

where $\hat{\mathbf{n}}$ is a unit vector perpendicular to the (100) surface. The average strain difference defined by Eq. (12) introduces an average change in GaAs symmetry from cubic to orthorhombic in a surface layer of thickness $\approx l$, thus leading to a reflectance anisotropy.

We note from Eq. (12) that only the edge component of the dislocation strain contributes to the average anisotropy, so that in what follows we will ignore the screw component.

D. RD line shapes

The reflectance-difference spectrum results from the contributions of all dislocations within the anisotropically strained layer of thickness l present at the surface of the semiconductor as discussed above. By assuming that the dislocation has an area of influence equal to $2l^2$, we may thus write for the RD line shape

$$\frac{\Delta R}{R} = 2l^2 p \sum_{ijk} \rho^{(ijk)} \, \text{Re}[(\alpha_s - i\beta_s)\Delta\varepsilon^{(ijk)}], \tag{13}$$

where α_s and β_s are Seraphin coefficients,[20] p is equal either to l or to the light penetration depth K^{-1}, whichever is smaller, and $\Delta\varepsilon^{(ijk)}$ for dislocation ijk is given by

$$\Delta\varepsilon^{(ijk)} \cong \hat{\mathbf{e}}_z \cdot \delta\varepsilon^{(ijk)} \cdot \hat{\mathbf{e}}_z - \hat{\mathbf{e}}_y \cdot \delta\varepsilon^{(ijk)} \cdot \hat{\mathbf{e}}_y, \tag{14}$$

where $\hat{\mathbf{e}}_y$ and $\hat{\mathbf{e}}_z$ are the light polarization vectors along [011] and [01̄1], respectively, and $\delta\varepsilon^{(ijk)}$ is the change in dielectric function under the presence of strain tensor (6a). In what follows we will obtain expressions for $\Delta\varepsilon^{(ijk)}$, for the Γ and Λ critical-point interband transitions studied in this paper.

1. E_0 and $E_0+\Delta_0$ transitions

The E_0 critical-point interband transition links the Γ_8 valence-band states $|\frac{3}{2}\frac{3}{2}\rangle$ and $|\frac{3}{2}\frac{1}{2}\rangle$ with the $|S\uparrow\rangle$ Γ_6 conduction-band states.[21] A surface anisotropy at E_0 arises because the strain tensor (6a) splits the valence band (see Fig. 5). Taking into account only terms linear in the stress, the total shift in energy ΔE_Γ for valence-band wave functions is given by (see Appendix A)
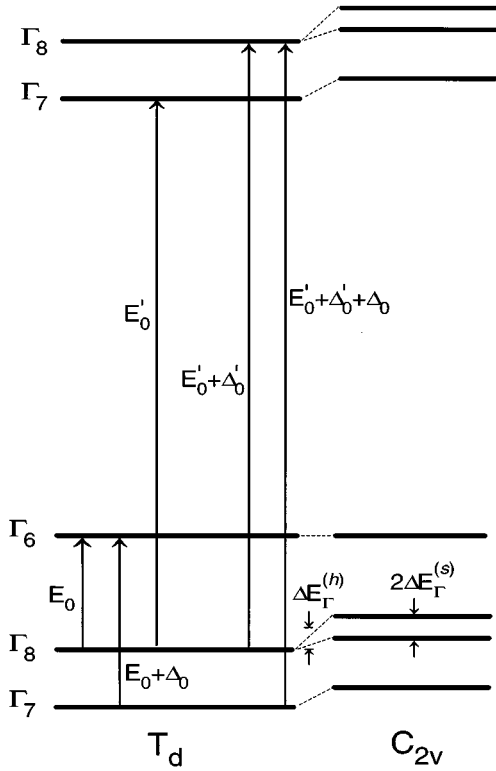
FIG. 5. Interband transitions in a zinc-blende crystal under a 60°
dislocation-induced strain. The change in crystal symmetry from
cubic (T_d) to orthorhombic (C_{2v}) leads to a hydrostatic shift $\Delta E_\Gamma^{(h)}$
and to a split energy $2\Delta E_\Gamma^{(s)}$ for the Γ^8 valence-band levels.

$$\Delta E_\Gamma = k\Delta E_\Gamma^{(h)} \pm k\Delta E_\Gamma^{(s)}$$

$$= ka\left(1 - \frac{c_{12}}{c_{11}}\right)\langle e_{22}\rangle \pm \frac{k}{2}\left[b^2\left(1 + 2\frac{c_{12}}{c_{11}}\right)^2 + d^2\right]^{1/2}\langle e_{22}\rangle,$$

$$(15)$$

where $\Delta E_\Gamma^{(h)}$ stands for the hydrostatic energy shift, $\Delta E_\Gamma^{(s)}$ is
half the valence-band-splitting energy, a, b, and d are the
deformation potentials for hydrostatic, tetragonal, and ortho-
rhombic deformations, respectively.

On the other hand, by neglecting the mixing of the Γ_8
wave functions with the Γ_7 spin-orbit split valence-band
states, we obtain the following differences in interband tran-
sition momentum matrix elements for $\hat{\mathbf{e}}_z$ and $\hat{\mathbf{e}}_y$ polarizations
(see Appendix A):

$$\Delta M_\Gamma^{(\pm)} = M_\Gamma^{(\pm)}(\hat{\mathbf{e}}_z) - M_\Gamma^{(\pm)}(\hat{\mathbf{e}}_y) = \pm\tfrac{3}{4}M_\Gamma(2\delta_{jk} - 1),$$

$$(16)$$

where

$$M_\Gamma = |\langle c|\mathbf{p}\cdot\hat{\mathbf{e}}|\nu\rangle|^2 \tag{17}$$

is the square of the momentum matrix element for E_0 tran-
sitions in the absence of strain, while of $M_\Gamma^{(\pm)}$ stands for the
square of the momentum matrix element for interband tran-
sitions involving upward and downward shifted valence-
band states, respectively.

To obtain an expression for $\delta\varepsilon^{(ijk)}$, we will make use of
the following expression for the unperturbed dielectric func-
tion

$$\varepsilon(E) = \frac{A}{E^2}M_\Gamma J(E), \tag{18}$$

where $J(E)$ is the joint density-of-states function for inter-
band transitions and A is a factor independent of energy.[22]

We note that $\delta\varepsilon^{(ijk)}$ is a diagonal tensor in the (x,y,z)
axis and that the two components relevant for us are $\delta\varepsilon_{22}^{(ijk)}$
and $\delta\varepsilon_{33}^{(ijk)}$, which may be written with the help of tensor
(6a) and Eq. (18) as

$$\delta\varepsilon_{33}^{(ijk)} = \frac{A}{E^2}\langle e_{22}\rangle[J(E + \Delta E_\Gamma^{(h)} + \Delta E_\Gamma^{(s)})M_\Gamma^{(+)}(\hat{\mathbf{e}}_z)$$

$$+ J(E + \Delta E_\Gamma^{(h)} - \Delta E_\Gamma^{(s)})M_\Gamma^{(-)}(\hat{\mathbf{e}}_z)], \tag{19a}$$

$$\delta\varepsilon_{22}^{(ijk)} = \frac{A}{E^2}\langle e_{22}\rangle[J(E + \Delta E_\Gamma^{(h)} + \Delta E_\Gamma^{(s)})M_\Gamma^{(+)}(\hat{\mathbf{e}}_y)$$

$$+ J(E + \Delta E_\Gamma^{(h)} - \Delta E_\Gamma^{(s)})M_\Gamma^{(-)}(\hat{\mathbf{e}}_y)]. \tag{19b}$$

From Eqs. (14), (16), and (19) we obtain

$$\Delta\varepsilon^{(ijk)} = \frac{A}{E^2}[\Delta M_\Gamma^{(+)}J(E + \Delta E_\Gamma^{(h)} + \Delta E_\Gamma^{(s)})$$

$$+ \Delta M_\Gamma^{(-)}J(E + \Delta E_\Gamma^{(h)} - \Delta E_\Gamma^{(s)})] \tag{20}$$

and, finally, from Eqs. (13), (18), and (20) we can write for
the RD line shape for the E_0 critical point

$$\frac{\Delta R}{R} = \frac{Cl^2}{2}p\Delta\rho\,\text{Re}\{(\alpha_s - i\beta_s)[\varepsilon(E_0 + \Delta E_\Gamma^{(h)} + \Delta E_\Gamma^{(s)})$$

$$- \varepsilon(E_0 + \Delta E_\Gamma^{(h)} - \Delta E_\Gamma^{(s)}) + \varepsilon(E_0 - \Delta E_\Gamma^{(h)} + \Delta E_\Gamma^{(s)})$$

$$- \varepsilon(E_0 - \Delta E_\Gamma^{(h)} - \Delta E_\Gamma^{(s)})]\}, \tag{21}$$

where $C = 3$. Furthermore, by assuming $\Delta E_\Gamma^{(s)} + \Delta E_\Gamma^{(h)} \ll \gamma$,
where γ is the line-shape broadening parameter, we obtain
from Eq. (21) the first derivative line shape

$$\frac{\Delta R}{R} = 2Cl^2p\Delta\rho\,\frac{1}{E^2}\,\text{Re}\left[(\alpha_s - i\beta_s)\left(\frac{\partial(E^2\varepsilon)}{\partial E}\right)\right]\Delta E_\Gamma^{(s)}. \tag{22}$$

Regarding the $E_0 + \Delta_0$ transitions, we note that by neglect-
ing the mixing of the Γ_8 and Γ_7 valence-band wave func-
tions, there is not any associated anisotropy, as the Γ_7
valence-band states are not split by the dislocation strain (see
Appendix A).

2. E_0' and $E_0' + \Delta_0' + \Delta_0$ transitions

The transitions that give rise to the E_0' optical structure of
GaAs are of the types $\Delta_5 \rightarrow \Delta_5$ and $\Gamma_8 \rightarrow \Gamma_7$.[23] We note, how-
ever, that the Δ transition is isotropic for light incidence on a
(100) surface and will be not be further considered. The
Γ-point E_0' interband transition links the fourfold-degenerate
Γ_8 valence-band states with the spin-degenerate Γ_7 upper
conduction-band states (see Fig. 5). Interband transition ma-
trix elements are thus given by Eq. (16), with M_Γ standing
for the E_0' transition matrix element for the unperturbed crys-
tal. In the same way, the RD line shape for the E_0' transition
is given by Eqs. (21) and (22).

Transition $E_0' + \Delta_0' + \Delta_0$ links the spin-orbit spliced valence-band Γ_7 levels with the upper conduction-band Γ_8 states,[23] as shown schematically in Fig. 5. As occurs for valence-band states, the strain tensor (6a) removes the energy degeneracy of the upper conduction-band levels Γ_8. We may thus expect that Eqs. (16), (20), and (21) are valid for this transition, with $\Delta E_\Gamma^{(s)}$ and $\Delta E_\Gamma^{(h)}$ standing for the upper conduction-band shifting energies and M_Γ for the $E_0' + \Delta_0' + \Delta_0$ transition matrix element in the absence of strain. Provided that $\Delta E_\Gamma^{(s)} + \Delta E_\Gamma^{(h)} \ll \gamma$ for this transition, the RD line shape is thus given by Eq. (22). We note, however, that we must include a *negative sign* in front of the second members of Eqs. (21) and (22), to take into account that in this case we are considering $\Gamma_7 \rightarrow \Gamma_8$ transitions instead of $\Gamma_8 \rightarrow \Gamma_7$.

3. $E_0' + \Delta_0'$ transitions

The $E_0' + \Delta_0'$ transition links fourfold-degenerate Γ_8 levels.[23] The calculation of the contribution of $E_0' + \Delta_0'$ to the RD spectrum is thus more complex than for the previous critical points, as it involves transitions between two strain-split sets of states (see Fig. 5). As discussed in Appendix A, however, matrix elements for these transitions can be neglected when compared with other Γ-point transitions.

4. E_1 and $E_1 + \Delta_1$ transitions

There are eight equivalent E_1 and $E_1 + \Delta_1$ critical points, corresponding, to the eight equivalent $\langle 111 \rangle$ directions in the Brillouin zone. E_1 and $E_1 + \Delta_1$ transitions link $|\Lambda_6^c\rangle$ conduction-band states with $|\Lambda_{4,5}\rangle$ and $|\Lambda_6^v\rangle$ valence-band states, respectively.[23] Under the influence of strain tensor (6a), the equivalence of both E_1 and $E_1 + \Delta_1$ critical points is removed, splitting $|\Lambda_6^c\rangle$ and $|\Lambda_{4,5}\rangle$ into states $|E_1^{(\pm)}\rangle$ and $|(E_1 + \Delta_1)^{(\mp)}\rangle$ (Ref. 21) with energy shifts given by (see Appendix B)

$$\Delta E_\Lambda = k \Delta E_\Lambda^{(h)} \pm k \Delta E_\Lambda^{(s)} = k(A^2 a + B^2 a')\left(1 - \frac{c_{12}}{c_{11}}\right)\langle e_{22}\rangle$$

$$\pm k \frac{1}{\sqrt{3}}\left(\frac{1}{2}d + B^2 d'\right)\langle e_{22}\rangle, \quad (23)$$

where a' and d' are the hydrostatic and orthorhombic deformation potentials for the conduction band, respectively, and $A = -B = 0.56$ for GaAs.[21]

Furthermore, by neglecting the mixing of the $|\Lambda_6^c\rangle$ and $|\Lambda_{4,5}\rangle$ bands ($\langle e_{22}\rangle/\Delta_1 \ll 1$), the dislocation strain leads to polarization selection rules that are expressed by the relationship (see Appendix B)

$$\Delta M_\Lambda^{(\pm)} = M_\Lambda^{(\pm)}(\hat{e}_z) - M_\Lambda^{(\pm)}(\hat{e}_y) = \pm M_\Lambda(1 - 2\delta_{jk}), \quad (24)$$

where $M_\Lambda^{(\pm)}$ stands for momentum matrix elements for interband transitions involving upward- and downward-shifted critical points, respectively, and M_Λ is the square of the momentum matrix element for interband transitions in the unperturbed crystal for both E_1 and $E_1 + \Delta_1$ transitions.

From the above discussion, an anisotropy at the E_1 and $E_1 + \Delta_1$ critical points arises for reasons similar to those for the Γ-point interband transitions. Thus, with the help of Eqs. (13) and (20), the RD line shape for the E_1 and $E_1 + \Delta_1$ critical points in first order in $\langle e_{22}\rangle$ is given by Eqs. (21) and
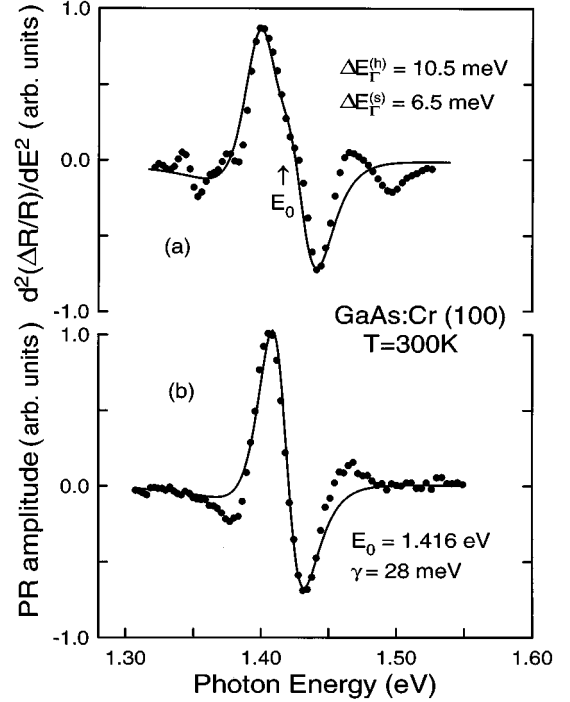
FIG. 6. (a) Second energy-derivative spectra of the RD line shape around the GaAs fundamental gap (filled circles) and line-shape fitting (continuous line). (b) Photoreflectance spectrum for GaAs:Cr (filled circles) and line-shape fitting (continuous line).

(22) with $C = -2$, provided that we substitute $\Delta E_\Gamma^{(h)}$ and $\Delta E_\Gamma^{(s)}$ with $\Delta E_\Lambda^{(h)}$ and $\Delta E_\Lambda^{(s)}$, respectively.

IV. DISCUSSION OF EXPERIMENTAL RESULTS

We will first consider results for the fundamental transition E_0. In order to isolate the dislocation-associated line shape of the RD spectrum of Fig. 2, we enhanced it against the relatively structureless background by taking its second derivative with respect to energy. Results are shown in Fig. 6(a). For the sake of comparison, in Fig. 6(b) we show a GaAs photoreflectance spectrum for the same sample as that employed in the RD measurements. The close coincidence between spectra of Figs. 6(a) and 6(b), constitutes further evidence of the existence of a first-derivative component in the RD line shape in accordance with our model, since photoreflectance line shapes are known to be associated with the third derivative of the reflectance spectra in the low-field regime.[24] We note, however, a shoulder in the RD spectrum that is not present in the PR line shape. This shoulder is due to the fact that for this particular sample condition $\Delta E_\Gamma^{(s)} + \Delta E_\Gamma^{(h)} \ll \gamma$ is not fulfilled. Thus, in this case the RD line shape is described by Eq. (21) rather than by Eq. (22).

By fitting the derived experimental RD spectrum in Fig. 6(a) to the second derivative of the theoretical model,[22] Eq. (21), we can obtain the numerical values for $\Delta E_\Gamma^{(h)}$ and $\Delta E_\Gamma^{(s)}$. Such a fitting is given by the continuous line spectrum in Fig. 6(a). We note that to build this spectrum we have made use of the fact that for the E_0 critical point of GaAs, $\Delta E_\Gamma^{(h)}/\Delta E_\Gamma^{(s)} \approx 1.62$. We have also employed the broadening energy $\gamma = 28$ meV and the gap energy $E_0 = 1.416$ eV obtained from the fitting of the photoreflectance (PR)
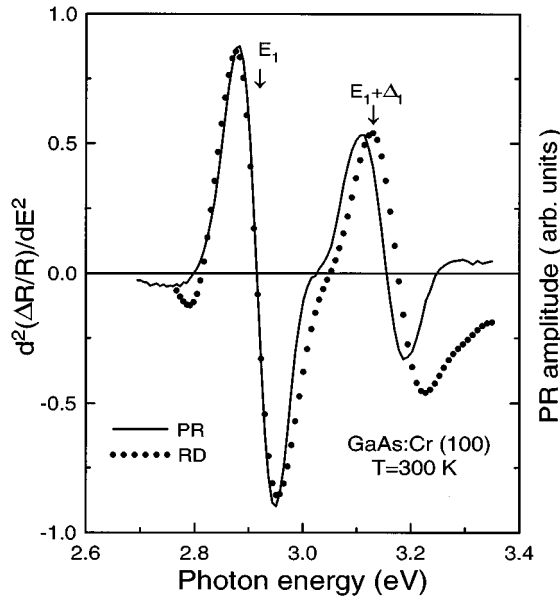
FIG. 7. Second energy-derivative spectra of the RD line shape around E_1 and $E_1 + \Delta_1$ (filled circles) and photoreflectance spectrum for undoped GaAs (continuous line).

experimental spectrum to a low-field M_0 line shape[22] [continuous line in Fig. 6(b)]. From the fitting of Fig. 6(a) we obtained $\Delta E_1^{(h)} = 10.5$ meV and $\Delta E_1^{(s)} = 6.5$ meV.

We note that from the fitting of the RD spectrum amplitude we can calculate the product $l^2 p \Delta \rho$, which, by assuming $p = l$ at E_0, allows us to determine the average change Δd_{eff} in lattice spacing along the $\langle 110 \rangle$ directions parallel to the surface. The absolute value of Δd_{eff} normalized to lattice spacing d is given by $|(\Delta d)_{\text{eff}}/d| = \langle e_{22} \rangle l^3 \Delta \rho$. The strain-tensor component $\langle e_{22} \rangle$ can be obtained from the $\Delta E_1^{(h)}$ and $\Delta E_1^{(s)}$ determined from the RD line-shape fitting. From the above we obtain $|(\Delta d)_{\text{eff}}/d|$ values in the range of $10^{-5} - 10^{-4}$ for our samples.

Regarding the contribution of the $E_0 + \Delta_0$ critical point to the RD spectrum, we can see from Fig. 2 that it is negligible, as anticipated in Sec. III D 1.

Let us now consider E_1 and $E_1 + \Delta_1$ transitions. Filled circles in Fig. 7 show the second derivative of the experimental RD spectra of our samples in the energy range around the E_1 and $E_1 + \Delta_1$ energies. In Fig. 7 we also show the PR spectrum of undoped GaAs (continuous line), which closely coincides with the RD spectrum of the same figure. In this case, due to the larger broadening energies as compared to transitions around the fundamental gap, the dislocation-induced component of the RD line shape is well described by a first-derivative line shape, in agreement with our model.

Regarding interband transitions above 4 eV, we note that in this case, both the larger broadening energies and the increased noise prevented us from obtaining meaningful spectrum energy derivatives. From Fig. 2, however, it appears that the contributions of the E_0' and $E_0' + \Delta_0' + \Delta_0$ transitions to the RD spectrum are about π radians out of phase with respect to each other, in accordance with the discussion of Sec. III D 2. Furthermore, the contribution of the $E_0' + \Delta_0'$ critical point to the RD spectrum appears to be negligible, a fact that also agrees with our model (Sec. III D 3).

We note that in GaAs the $E_0' + \Delta_0' + \Delta_0$ transition is almost degenerate with the transition labeled E_2, and that the broadening of the RD spectrum of Fig. 2 makes it difficult to resolve both transitions. However, and although the symmetry of the E_2 is unknown,[23] we can see from Fig. 2 that the contribution of the E_2 transition to the RD line shape has the same phase as that of $E_0' + \Delta_0' + \Delta_0$.

Furthermore, we note that the relative phases of the E_1 and $E_1 + \Delta_1$ critical-point components in the RD spectra of Fig. 2 with respect to the corresponding phases for the E_0' and $E_0' + \Delta_0' + \Delta_0$ components are congruent with the predictions of our model (Secs. III D 2 and III D 4). This is, however, not the case for the E_0-point component, whose RD line shape is predicted to be π radians out of phase with respect to that observed experimentally (see Sec. III D 1). This may be associated with the fact that around the fundamental gap the light penetration depth (a few micrometers) is two orders of magnitude larger than the penetration depth at higher energies, that is, 100–200 Å. Thus, at high energies we are actually sensing a region that is different from that sensed by photons around E_0, each region having its own distribution of dislocations. We may expect that for the RD spectrum around E_0 the line shape is associated with dislocations formed during crystal growth, while at higher energies the RD line shape is to a great extent determined by sample surface preparation.

As an additional mechanism to help understand the above phase discrepancy, we note that the inhomogeneity along x of the average strain field Eq. (3) may introduce a shift in the phase of the RD line shape. Such a phase shift is a function of the dislocation-length–to–light-penetration-depth ratio and is largest around E_0. The effect of a spatial inhomogeneity in the perturbation field in modulated reflectance line shapes has been considered by various authors.[25,26] Aspnes and Frova[25] have shown that for light-penetration depths large compared to the thickness of the inhomogeneous perturbation, substantial modifications in the modulated reflectance line shape are obtained as compared to the line shape for a homogeneous perturbation. In a similar way, Behn and Roppischer[26] report on both theoretical and experimental electroreflectance spectra showing dramatic changes in spectral line shapes as a function of bias voltage. If the observed phase discrepancies in the RD spectrum were entirely due to the strain-field inhomogeneity, the difference in phase factors for energies around E_0 and E_1 should be $\approx \pi$. Work is under way in an attempt to settle this issue.

V. CONCLUSIONS

We have developed a model to describe RD spectra for the (100) surface of zinc-blende semiconductors due to strains induced by α and β 60° dislocations. The model takes into account the strain contributions of all α and β dislocations present within the penetration depth of the light. Provided that we have a difference in α and β dislocation densities, it is shown that such contributions result in an anisotropic average strain near the semiconductor surface that changes the sample symmetry from cubic to orthorhombic, thus leading to a reflectance anisotropy. The model predicts RD line shapes for critical points of both Γ and Λ symmetry that are proportional to the first energy derivative

of the reflectance spectrum as long as the strain-induced energy shifts are small compared to the spectrum broadening energies. The overall RD spectrum is predicted to be a linear combination of the individual line shapes associated with each critical point. The amplitude and phase of each of these line shapes in the linear combination are dependent on the specific critical point considered. We presented RD spectra of semi-insulating (100) GaAs:Cr in the 1.2–5.5-eV energy range that confirm the predictions of our model.

ACKNOWLEDGMENTS

APPENDIX A

We will consider in this appendix the effect of the dislocation-induced strains on the anisotropy of E_0 ($\Gamma_8 \rightarrow \Gamma_6$), $E_0 + \Delta_0$ ($\Gamma_7 \rightarrow \Gamma_6$), and $E_0' + \Delta_0'$ ($\Gamma_8 \rightarrow \Gamma_8$) critical-point interband transitions. We will choose coordinated axis x', y', z' along [100], [010], and [001], respectively. Let us first consider E_0 and $E_0 + \Delta_0$. The conduction-band Γ_6 wave functions are $|S\uparrow\rangle$ and $|S\downarrow\rangle$. The valence-band states of Γ_8 symmetry can be written as[21]

$$\left|\frac{3}{2}\,\frac{3}{2}\right\rangle^{(jk)} = \frac{1}{\sqrt{2}}\left(x' + i\,\frac{1}{\sqrt{2}}\,(z' - jky')\right)|\uparrow\rangle, \quad \text{(A1a)}$$

$$\left|\frac{3}{2}-\frac{3}{2}\right\rangle^{(jk)} = \frac{1}{\sqrt{2}}\left(x' - i\,\frac{1}{\sqrt{2}}\,(z' - jky')\right)|\downarrow\rangle, \quad \text{(A1b)}$$

$$\left|\frac{3}{2}\,\frac{1}{2}\right\rangle^{(jk)} = \frac{1}{\sqrt{3}}\,(z' + jky')|\uparrow\rangle$$
$$- \frac{1}{\sqrt{6}}\left(x' + i\,\frac{1}{\sqrt{2}}\,(z' - jky')\right)|\downarrow\rangle, \quad \text{(A1c)}$$

$$\left|\frac{3}{2}-\frac{1}{2}\right\rangle^{(jk)} = \frac{1}{\sqrt{3}}\,(z' + jky')|\downarrow\rangle$$
$$+ \frac{1}{\sqrt{6}}\left(x' - \mathbf{i}\,\frac{1}{\sqrt{2}}\,(z' - jky')\right)|\uparrow\rangle, \quad \text{(A1d)}$$

while the spin-orbit-split Γ_7 valence-band states are given by[21]

$$\left|\frac{1}{2}\,\frac{1}{2}\right\rangle^{(jk)} = \frac{1}{\sqrt{6}}\,(z' + jky')|\uparrow\rangle$$
$$+ \frac{1}{\sqrt{3}}\left(x' + i\,\frac{1}{\sqrt{2}}\,(z' - jky')\right)|\downarrow\rangle, \quad \text{(A2a)}$$

$$\left|\frac{1}{2}-\frac{1}{2}\right\rangle^{(jk)} = \frac{1}{6}\,(z' + jky')|\downarrow\rangle$$
$$- \frac{1}{\sqrt{3}}\left(x' - i\,\frac{1}{\sqrt{2}}\,(z' - jky')\right)|\uparrow\rangle. \quad \text{(A2b)}$$

The Hamiltonian describing the combined spin-orbit and elastic interactions of the dislocation-induced strain tensor (6a) with the crystal can be written[21]

$$H = -a\langle e_{22}\rangle k\left[1 - \frac{c_{12}}{c_{11}}\right] - \frac{3}{2}\,b\langle e_{22}\rangle k\left[-2\frac{c_{12}}{c_{11}}\,L_{x'}^2 + L_{y'}^2 + L_{z'}^2\right.$$
$$+ \frac{2}{3}\left(\frac{c_{12}}{c_{11}} - 1\right)\mathbf{L}^2\right] - \sqrt{3}d\langle e_{22}\rangle k\,\frac{(L_{y'}L_{z'} + L_{z'}L_{y'})}{2}$$
$$+ \kappa\mathbf{L}\cdot\mathbf{S}, \quad \text{(A3)}$$

where $\mathbf{L}$ is the angular momentum, a, b, and d are the deformation potentials for hydrostatic, tetragonal, and orthorhombic deformations, respectively, and $\kappa = \Delta_0/3$.

Valence-band eigenvectors of Hamiltonian (A3) are a mixture of Γ_7 and Γ_8 states and are written as

$$|E_0^{(+)}\rangle = \lambda\left|\frac{3}{2},\frac{3}{2}\right\rangle^{(jk)} + \mu\left|\frac{3}{2},-\frac{1}{2}\right\rangle^{(jk)}$$
$$+ \sqrt{2}\,\eta\,\frac{\langle e_{22}\rangle}{\Delta_0}\left|\frac{1}{2},-\frac{1}{2}\right\rangle^{(jk)}, \quad \text{(A4a)}$$

$$|E_0^{(-)}\rangle = \lambda\left|\frac{3}{2},-\frac{1}{2}\right\rangle^{(jk)} - \mu\left|\frac{3}{2},\frac{3}{2}\right\rangle^{(jk)}$$
$$+ \frac{\xi}{\sqrt{2}}\,\frac{\langle e_{22}\rangle}{\Delta_0}\left|\frac{1}{2},-\frac{1}{2}\right\rangle^{(jk)}, \quad \text{(A4b)}$$

$$|E_0 + \Delta_0\rangle = \left|\frac{1}{2},-\frac{1}{2}\right\rangle^{(jk)} - \frac{\xi}{\sqrt{2}}\,\frac{\langle e_{22}\rangle}{\Delta_0}\left|\frac{3}{2},-\frac{1}{2}\right\rangle^{(jk)}$$
$$- \sqrt{2}\,\eta\,\frac{\langle e_{22}\rangle}{\Delta_0}\left|\frac{3}{2},\frac{3}{2}\right\rangle^{(jk)}, \quad \text{(A4c)}$$

where

$$\lambda = \frac{\eta}{\{\eta^2 + [\xi - (\xi^2 + \eta^2)^{1/2}]^2\}^{1/2}}, \quad \text{(A4d)}$$

$$\eta = \frac{\sqrt{3}}{4}\left[b\left(1 + 2\frac{c_{12}}{c_{11}}\right) - \frac{d}{\sqrt{3}}\right], \quad \text{(A4e)}$$

$$\xi = \frac{1}{4}\left[b\left(1 + 2\frac{c_{12}}{c_{11}}\right) + \sqrt{3}d\right], \quad \text{(A4f)}$$

and

$$\lambda^2 + \mu^2 = 1. \tag{A4g}$$

From the above eigenvectors, we obtain the energy shifts for states $|E_0^{(\pm)}\rangle$ given by Eq. (15), as well as the following interband matrix elements:

$$|\langle S\uparrow|\mathbf{p}\cdot\hat{\mathbf{e}}_y|E_0^{(-)}\rangle|^2 = M_\Gamma^{(-)}(\hat{\mathbf{e}}_y)$$

$$= M_\Gamma \left\{ \left[\lambda^2 + \lambda\xi \frac{\langle e_{22}\rangle}{\Delta_0} \right] \delta_{jk} \right.$$

$$+ \left[\frac{1}{4}\lambda^2 - \frac{\sqrt{3}}{2}\lambda\mu - \frac{1}{2}\lambda\xi \frac{\langle e_{22}\rangle}{\Delta_0} \right]$$

$$\left. \times (1 - \delta_{jk}) \right\}, \tag{A5a}$$

$$|\langle S\uparrow|\mathbf{p}\cdot\hat{\mathbf{e}}_z|E_0^{(-)}\rangle|^2 = M_\Gamma^{(-)}(\hat{\mathbf{e}}_z)$$

$$= M_\Gamma \left\{ \left[\frac{1}{4}\lambda^2 - \frac{\sqrt{3}}{2}\lambda\mu - \frac{1}{2}\lambda\xi \frac{\langle e_{22}\rangle}{\Delta_0} \right] \delta_{jk} \right.$$

$$\left. + \left[\lambda^2 + \lambda\xi \frac{\langle e_{22}\rangle}{\Delta_0} \right] (1 - \delta_{jk}) \right\}, \tag{A5b}$$

$$|\langle S\uparrow|\mathbf{p}\cdot\hat{\mathbf{e}}_y|E_0^{(+)}\rangle|^2 = M_\Gamma^{(+)}(\hat{\mathbf{e}}_y)$$

$$= M_\Gamma \left\{ 2\mu\eta \frac{\langle e_{22}\rangle}{\Delta_0} \delta_{jk} \right.$$

$$+ \left[\frac{3}{4}\lambda^2 + \frac{\sqrt{3}}{2}\lambda\mu - \sqrt{3}\lambda\eta \frac{\langle e_{22}\rangle}{\Delta_0} \right]$$

$$\left. \times (1 - \delta_{jk}) \right\}, \tag{A5c}$$

$$|\langle S\uparrow|\mathbf{p}\cdot\hat{\mathbf{e}}_z|E_0^{(+)}\rangle|^2 = M_\Gamma^{(+)}(\hat{\mathbf{e}}_z)$$

$$= M_\Gamma \left\{ \left[\frac{3}{4}\lambda^2 + \frac{\sqrt{3}}{2}\lambda\mu - \sqrt{3}\lambda\eta \frac{\langle e_{22}\rangle}{\Delta_0} \right] \delta_{jk} \right.$$

$$\left. + 2\mu\eta \frac{\langle e_{22}\rangle}{\Delta_0} (1 - \delta_{jk}) \right\}, \tag{A5d}$$

$$|\langle S\uparrow|\mathbf{p}\cdot\hat{\mathbf{e}}_y|E_0+\Delta_0\rangle|^2 = M_\Gamma \left\{ \left[1 + 2\xi \frac{\langle e_{22}\rangle}{\Delta_0} \right] \delta_{jk} \right.$$

$$\left. + \left[1 - \xi \frac{\langle e_{22}\rangle}{\Delta_0} \right] (1 - \delta_{jk}) \right\}, \tag{A5e}$$

$$|\langle S\uparrow|\mathbf{p}\cdot\hat{\mathbf{e}}_z|E_0+\Delta_0\rangle|^2 = M_\Gamma \left\{ \left[1 - \xi \frac{\langle e_{22}\rangle}{\Delta_0} \right] \delta_{jk} \right.$$

$$\left. + \left[1 + 2\xi \frac{\langle e_{22}\rangle}{\Delta_0} \right] (1 - \delta_{jk}) \right\}, \tag{A5f}$$

where $\hat{\mathbf{e}}_y$ and $\hat{\mathbf{e}}_z$ are polarization vectors along [011] and [0$\bar{1}$1], respectively, and M_Γ is the square matrix element in the absence of strain.

Taking into account that $\mu \approx 0.05\lambda$ for GaAs, we can neglect in the first approximation terms depending on μ in Eqs.

(A5). In this way, by making $\lambda = 1$ and by neglecting any mixing of the valence-band Γ_8 wave functions with the spin-orbit-split Γ_7 states (i.e., by assuming $\langle e_{22}\rangle/\Delta_0 \ll 1$), we obtain from Eqs. (A5) the differences $\Delta M_\Gamma^{(\pm)}$ given in Eq. (16).

On the other hand, from Eqs. (A5e) and (A5f) we can see that by neglecting any mixing of the valence-band Γ_8 and Γ_7 wave functions, the interband transitions involving $|E_0+\Delta_0\rangle$ states do not contribute to RD spectra.

We will now consider the $E_0'+\Delta_0'$ ($\Gamma_8 \rightarrow \Gamma_8$) interband transition. As discussed above, each one of the states involved in this transition are split by the dislocation strain into two states. These two states will be termed $\Psi^{(\pm)}$, where plus and minus signs stand for upward- and downward-shifted states, respectively. In the perturbed crystal, four different interband transitions are then possible, with Eqs. (A2) and Hamiltonian (B3) leading to the following interband matrix elements:

$$\langle\Psi^{(\pm)}|\mathbf{p}\cdot\hat{\mathbf{e}}_y|\Psi^{(\pm)}\rangle = \tfrac{4}{3}Q^2\lambda^2\mu^2\delta_{jk}, \tag{A6a}$$

$$\langle\Psi^{(\pm)}|\mathbf{p}\cdot\hat{\mathbf{e}}_y|\Psi^{(\mp)}\rangle = \tfrac{1}{3}Q^2(\lambda^2-\mu^2)^2\delta_{jk} + \tfrac{1}{3}Q^2(\lambda^2+\mu^2)^2$$

$$\times (1 - \delta_{kj}), \tag{A6b}$$

$$\langle\Psi^{(\pm)}|\mathbf{p}\cdot\hat{\mathbf{e}}_z|\Psi^{(\pm)}\rangle = \tfrac{4}{3}Q^2\lambda^2\mu^2(1 - \delta_{kj}), \tag{A6c}$$

$$\langle\Psi^{(\pm)}|\mathbf{p}\cdot\hat{\mathbf{e}}_z|\Psi^{(\mp)}\rangle = \tfrac{1}{3}Q^2(\lambda^2+\mu^2)^2\delta_{kj} + \tfrac{1}{3}(\lambda^2-\mu^2)^2$$

$$\times (1 - \delta_{kj}). \tag{A6d}$$

As can be seen from Eqs. (A6), differences in matrix elements for polarizations $\hat{\mathbf{e}}_y$ and $\hat{\mathbf{e}}_z$ for a given interband transition are either zero or of second order in μ. Thus, $E_0'+\Delta_0'$ transitions contribute only in second order to the RD line shape and will be neglected.

APPENDIX B

We will consider interband transitions at the E_1 ($\Lambda_{4,5} \rightarrow \Lambda_6$) and $E_1+\Delta_1$ ($\Lambda_6 \rightarrow \Lambda_6$) critical points, which involve the conduction-band wave functions[21]

$$|\Lambda_6^c\rangle^{(jk)} = A|S\uparrow\rangle + \frac{B}{\sqrt{3}}(\pm jk(x'\pm y') + z')|\uparrow\rangle \tag{B1}$$

and the valence-band wave functions[21]

$$|\Lambda_{4,5}\rangle^{(jk)} = \frac{1}{2}\left[z' \mp jky' + i\frac{1}{\sqrt{3}}(z' \pm jk(y'-2x')) \right]|\uparrow\rangle, \tag{B2a}$$

$$|\Lambda_6^v\rangle^{(jk)} = \frac{1}{2}\left[z' \mp jky' - i\frac{1}{\sqrt{3}}(z' \pm jk(y'-2x')) \right]|\uparrow\rangle, \tag{B2b}$$

where the upper and lower signs stand for the [111] and [11$\bar{1}$] bands, respectively. The Hamiltonian (A3), with $\kappa = \sqrt{3}\Delta_1/2$, is still appropriate for describing the strain interaction at the Λ points, as the term $\mathbf{k}\cdot\mathbf{p}$ is not dependent on strain in first order.[21] The eigenvectors of Hamiltonian (A3) are given by

$$|E_1^{(\pm)}\rangle = |\Lambda_{4,5}\rangle^{(jk)} \pm \zeta \frac{\langle e_{22}\rangle}{\Delta_1} |\Lambda_6^\nu\rangle^{(jk)}, \qquad \text{(B3a)}$$

$$|(E_1+\Delta_1)^{(\mp)}\rangle = |\Lambda_6^\nu\rangle^{(jk)} \mp \zeta \frac{\langle e_{22}\rangle}{\Delta_1} |\Lambda_{4,5}\rangle^{(jk)}, \quad \text{(B3b)}$$

where plus and minus signs stand for upward- and downward-shifted critical points, respectively, and

$$\zeta = \left[\frac{d}{\sqrt{3}} - b\left(\frac{1}{2} + \frac{c_{12}}{c_{11}}\right)\right]. \qquad \text{(B4)}$$

Hamiltonian (A3) and eigenvectors (B3) lead to the energy splittings given in Eq. (23), as well as to the interband momentum matrix elements

$$|\langle \Lambda_6^c | \mathbf{p} \cdot \hat{\mathbf{e}}_y | E_1^{(\pm)}\rangle|^2 = M_\Lambda^{(\pm)}(\hat{\mathbf{e}}_y)$$
$$= \frac{M_\Lambda^2}{2}\left[(2\mp 1)\left(1 - r\,\frac{1}{2}\,\zeta\,\frac{\langle e_{22}\rangle}{\Delta_1}\right)\delta_{jk}\right.$$
$$\left. + (2\pm 1)\left(1 + r\,\frac{1}{2}\,\zeta\,\frac{\langle e_{22}\rangle}{\Delta_1}\right)(1-\delta_{jk})\right],$$
$$\text{(B5a)}$$

$$|\langle \Lambda_6^c | \mathbf{p} \cdot \hat{\mathbf{e}}_z | E_1^{(\pm)}\rangle|^2 = M_\Lambda^{(\pm)}(\hat{\mathbf{e}}_z)$$
$$= \frac{M_\Lambda^2}{2}\left[(2\pm 1)\left(1 + r\,\frac{1}{2}\,\zeta\,\frac{\langle e_{22}\rangle}{\Delta_1}\right)\delta_{jk}\right.$$
$$\left. + (2\mp 1)\left(1 - r\,\frac{1}{2}\,\zeta\,\frac{\langle e_{22}\rangle}{\Delta_1}\right)(1-\delta_{jk})\right],$$
$$\text{(B5b)}$$

where $r=1$ and M_Λ is the square of the momentum matrix element for interband transitions in the unperturbed crystal. Equations (B5a) and (B5b) also apply for transitions involving the $|(E_1+\Delta_1)^{(\mp)}\rangle$ states with $r=-1$.

From Eqs. (B5a) and (B5b) we obtain the following differences in matrix elements for $\hat{\mathbf{e}}_y$ and $\hat{\mathbf{e}}_z$ polarizations for transitions involving both $|E_1^\mp\rangle$ and $|(E_1+\Delta_1)^{(\mp)}\rangle$ states:

$$\Delta M_\Lambda^{(\pm)} = M_\Lambda^{(\pm)}(\hat{\mathbf{e}}_z) - M_\Lambda^{(\pm)}(\hat{\mathbf{e}}_y)$$
$$= M_\Lambda\left(1 \pm r\zeta\,\frac{\langle e_{22}\rangle}{\Delta_1}\right)(1 - 2\delta_{jk}), \qquad \text{(B6)}$$

where Δ_1 is the spin-orbit interaction energy. Finally, by neglecting the mixing of the $|\Lambda_6^\nu\rangle$ and $|\Lambda_{4,5}\rangle$ states we obtain Eq. (24).

[1] D. E. Aspnes and A. A. Studna, Phys. Rev. Lett. **54**, 1956 (1985).

[2] D. E. Aspnes, J. P. Harbison, A. A. Studna, L. T. Florez, and M. K. Kelly, J. Vac. Sci. Technol. B **6**, 1127 (1988).

[3] D. E. Aspnes, E. Colas, A. A. Studna, R. Bhat, M. A. Koza, and V. G. Keramidas, Phys. Rev. Lett. **61**, 2782 (1988).

[4] H. Tanaka, E. Colas, A. A. Studna, D. E. Aspnes, and R. Bhat, Appl. Phys, Lett. **59**, 3443 (1991).

[5] D. E. Aspnes, J. Vac. Sci. Technol. B **3**, 1498 (1985).

[6] R. Del Sole, W. L. Mochan, and R. G. Barrera, Phys. Rev. B **43**, 2136 (1991).

[7] W. L. Mochán and R. G. Barrera, Phys. Rev. Lett. **55**, 1192 (1985).

[8] D. E. Aspnes and A. A. Studna, J. Vac. Sci. Technol. A **5**, 546 (1987).

[9] Y. C. Chang, S. F. Ren, and D. E. Aspnes, J. Vac. Sci. Technol. A **10**, 1856 (1992).

[10] S. E. Acosta-Ortíz and A. Lastras-Martínez, Phys. Rev. B **40**, 1426 (1989).

[11] S. E. Acosta Ortíz and A. Lastras-Martínez, Proc. SPIE **1286**, 31 (1990).

[12] L. F. Lastras-Martínez and A. Lastras-Martínez, Solid State Commun. **98**, 479 (1996).

[13] S. E. Acosta-Ortíz and A. Lastras-Martínez, Solid State Commun. **64**, 809 (1987).

[14] L. F. Lastras-Martínez, A. Lastras-Martínez, and R. E. Balderas-Navarro, Rev. Sci. Instrum. **64**, 2147 (1993).

[15] I. Yonenaga and K. Sumino, J. Appl. Phys. **65**, 85 (1989).

[16] M. S. Abrahams, J. Blanc, and C. J. Buiocchi, Appl. Phys. Lett. **21**, 185 (1972).

[17] See, e.g., J. P. Hirth and J. Lothe, *Theory of Dislocations* (Krieger, Malabar, FL, 1992), p. 373.

[18] J. D. Eshelby, W. T. Read, and W. Shockley, Acta Metal. **1**, 251 (1953).

[19] See e.g., L. D. Landau and E. M. Lifshitz, *Course of Theoretical Physics* (Pergamon, Oxford, 1986), Vol. 7, p. 113.

[20] See, e.g., D. E. Aspnes, in *Handbook on Semiconductors*, edited by M. Balkanski (North Holland, Amsterdam, 1980), Vol. 2, p. 121.

[21] F. H. Pollak and M. Cardona, Phys. Rev. **172**, 816 (1968).

[22] See, e.g., D. E. Aspnes, in *Handbook on Semiconductors* (Ref. 20), p. 125.

[23] D. E. Aspnes and A. A. Studna, Phys. Rev. B **7**, 4605 (1973).

[24] D. E. Aspnes, Surf. Sci. **37**, 418 (1973).

[25] D. E. Aspnes and A. Frova, Solid State Commun. **7**, 155 (1969).

[26] U. Bhen and H. Roppischer, J. Phys. C **21**, 5507 (1988).